# Hyperon Physics with PANDA at FAIR

Karin Schönning[1,*] for the PANDA collaboration

[1]Department of Physics and Astronomy, Uppsala University, Sweden

**Abstract.**
Hyperons provide new angles on two of the most challenging problems in contemporary physics: a coherent and quantitative description of the strong interaction, and the matter-antimatter asymmetry of the Universe. The production dynamics and the electromagnetic structure of strange hyperons, as well as hyperon spectroscopy, give insights into the strong interaction in the confinement domain. Furthermore, two-body decays of strange hyperons provide clean tests of CP symmetry, an essential piece to the matter-antimatter puzzle. The future experiment PANDA at FAIR offers unique possibilities to study different aspects of hyperons using antiproton beams. In particular, the hitherto almost unexplored multi-strange sector will be addressed. The expected large production cross sections of hyperons and the versatile, near 4 $\pi$ detector design makes PANDA a veritable hyperon factory already from the first phase of operation. In these proceedings, the opportunities for hyperon physics with PANDA will be outlined. I will also address how we can benefit from the weak hyperon decays, that provide straight-forward access to the full spin density matrix.

## 1 Introduction

In this proceedings, I will outline how hyperons can shed light on some of the most challenging, unresolved problems of contemporary physics. These problems are all related to one of the most abundant building blocks of the Universe: the nucleon.

Despite being known for a century, many of the nucleon features remain a mystery. Until this day, we are struggling to understand from first principles (a) its abundance, (b) its spin, (c) its mass, (d) its intrinsic structure and (e) its size: (a) There is much more matter (nucleons) than anti-matter (anti-nucleons) in the Universe. If this was not fine-tuned at the Big Bang, then this asymmetry must be of dynamical origin [1]. (b) The sum of the measured valence quarks' contribution to the nucleon spin is only about half of the total spin [2]. (c) In the chiral limit, where the (current) quark masses are zero, the mass of the resulting nucleon would still amount to more than 90% of the physical nucleon mass [3]. Thus, in contrast to the electron, the nucleon mass is not governed by the Higgs mechanism, but is dynamically generated of the strong interaction. To phrase it differently: More than 90% of the visible mass of the Universe is caused by the strong interaction. (d) The neutron has an intriguing charge distribution: negative in the center and at the rim, positive in between [4]. For a ground-state wave function this amount of wiggles is surprising. (e) The electric radius of the proton has been determined from electron-proton scattering, from the spectrum of electronic hydrogen and from the spectrum of muonic hydrogen. Most measurements using electrons resulted in a larger proton radius than the results obtained with muons [5]. This is known as the proton radius puzzle which puts lepton universality into question. In a recent measurement of electronic hydrogen, a smaller radius was obtained that was in agreement with measurements with muons [6]. However, the internal disagreements of the electron data remain to be understood.

A successful approach in various areas of physics when you do not understand a system, is to make a small change and see how it reacts. For instance[7]

1. Scatter on it
2. Excite it
3. Replace one of the building blocks

In these proceedings, we will focus on the third item. Replacing a building block – in this case a light quark – in a nucleon with a different one – a strange, charm or bottom quark – results in a hyperon. The question *"What happens if you replace one of the light quarks in a nucleon, with a heavier one?"* constitutes the common ground of hyperon physics. By combining two or three of the items, research fields such as hyperon structure (item 1 and 3) and hyperon spectroscopy (item 2 and 3) emerge.

## 2 Hyperons

The scale probed in a given reaction depends on the mass of the interacting entities. In the production of a system with strangeness, the scale is governed by the mass of the strange quark, $m_s \approx 95$ MeV/$c^2$ which is close to the cut-off $\Lambda_{QCD} \approx 200$ MeV/c$^2$, defining the scale where quarks are confined into composite systems. As a consequence,

*e-mail: karin.schonning@physics.uu.se

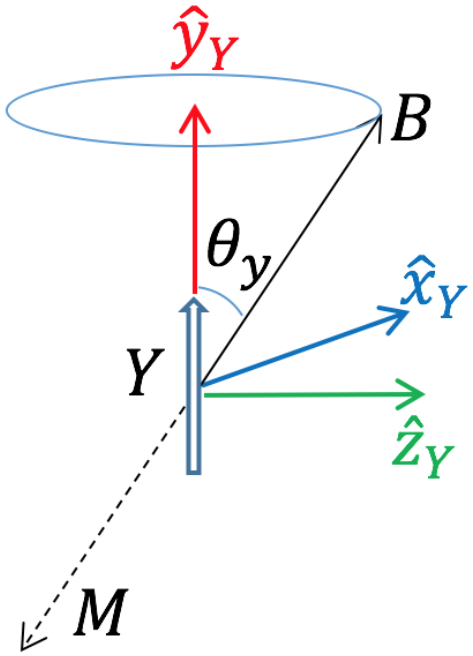


**Figure 1.** The $Y \rightarrow BM$ decay, with the spin direction of $Y$ along the $y$-axis.

the relevant degrees of freedom of such processes are unclear: quarks and gluons, or hadrons? Strange hadrons, *e.g.* hyperons, therefore probe the confinement domain of the strong interaction. This is in contrast to the charm quark /$m_c \approx 1275$ MeV/$c^2$) which is more than ten times heavier than the strange quark. This corresponds to the scale where perturbative QCD breaks down and these processes therefore probe the transition region between perturbative and non-perturbative QCD.

Hyperons have an advantage compared to nucleons: their weak, parity violating and thereby self-analysing decays. This means that the daughter particles from a hyperon decay are emitted according to the direction of the spin of the mother hyperon. Figure 1 illustrates the two-body decay $Y \rightarrow BM$, where a spin 1/2 hyperon $Y$ decays into a spin 1/2 baryon $B$ and a pseudo-scalar meson $M$. The angular distribution $W(\cos\theta_B)$ of $B$ in the rest system of $Y$ can be expressed in terms of the polarisation $P_y(\cos\theta_Y)$ with respect to some reference axis $\vec{y}$ as a function of the $Y$ scattering angle [8, 9]

$$W(\cos\theta_B) = \frac{1}{4\pi}(1 + \alpha P_y(\cos\theta_Y)\cos\theta_B). \qquad (1)$$

$P_y$ carries information about the production process and depends on the energy. The decay asymmetry $\alpha$ is related to the interference between the parity violating and the parity conserving decay amplitudes, $T_s$ and $T_p$ [10]. Equation 1 shows how parameters with physical meaning can be extracted from measurable quantities and demonstrates the unique potential of the hyperon as a diagnostic tool.

## 3 PANDA at FAIR

The future experiment Proton antiproton ANnihilations at DArmstadt (PANDA) at the Facility for Antiproton and Ion Research (FAIR) in Darmstadt, Germany, offers unique opportunities for hyperon physics. PANDA will be an integrated part of the High Energy Storage Ring (HESR). It is a multipurpose detector designed for a broad physics program, with focus on the strong interaction [11].

### 3.1 The HESR

The antiprotons will be delivered from the HESR within a momentum range from 1.5 GeV/$c$ up to 15 GeV/$c$. In the start-up phase, or *Phase One*, the HESR will be able to accumulate up to $10^{10}$ antiprotons within a time span of 1000 s. In a final stage, *Phase Three*, a dedicated ring *i.e.* the Recuperated Experimental Storage Ring (RESR) will allow up to $10^{11}$ antiprotons to be injected and stored in the HESR. HESR offers stochastic cooling that results in a beam momentum spread of better than $5 \cdot 10^{-5}$. The antiproton beam will impinge on a hydrogen cluster jet or pellet target. During the Phase One, the HESR will provide a luminosity of $\approx 10^{31}\ cm^2 s^{-1}$ whilst the design luminosity of $\approx 2 * 10^{32}\ cm^2 s^{-1}$ will be achieved during Phase Three.

### 3.2 The PANDA detector

The PANDA detector [11] is divided into a target spectrometer part (TS) and a forward spectrometer part (FS). The TS provide precise vertex tracking by the micro vertex detector (MVD), straw tube trackers (STT) and gas electron multiplier detectors (GEM). Time-of-flight detectors (TOF) and detection of internally reflected Cherenkov light (DIRC) offer particle identification and an electromagnetic calorimeter (EMC) will measure energies. The trajectories in the TS are bent by the field of a solenoid magnet providing a field of 2.0 T. The FS consists of straw tube stations for tracking, a dipole magnet, a ring imaging Cherenkov counter (RICH) detector and a TOF for particle identification and a Shashlyk electromagnetic calorimeter. The PANDA detector is shown in Fig. 3.

PANDA will be one of the first experiments featuring a time-based data acquisition system (DAQ) where data are read out as a continuous stream using an entirely software-based data selection scheme. This is in contrast to the present paradigm where data are acquired from the detectors by means of a hardware trigger. This change of paradigm is driven by the increasing reaction rates and large amounts of data to be stored. However, the software filter will provide a challenge since it needs to reconstruct events, tracks and clusters in real time to make decisions. At the design luminosity, the event rate will be up to 20 MHz which requires solutions beyond the state of the art in data processing and transmission.

The feasibility studies as well as future data analysis are performed within the common simulation and analysis framework PandaROOT [12]. It comprises the complete simulation chain, including Monte Carlo event generation, particle propagation and detector response, hardware digitization, reconstruction and calibration, and data analysis. PandaROOT is derived from the FairROOT framework [13] which in turn is based on ROOT [14].

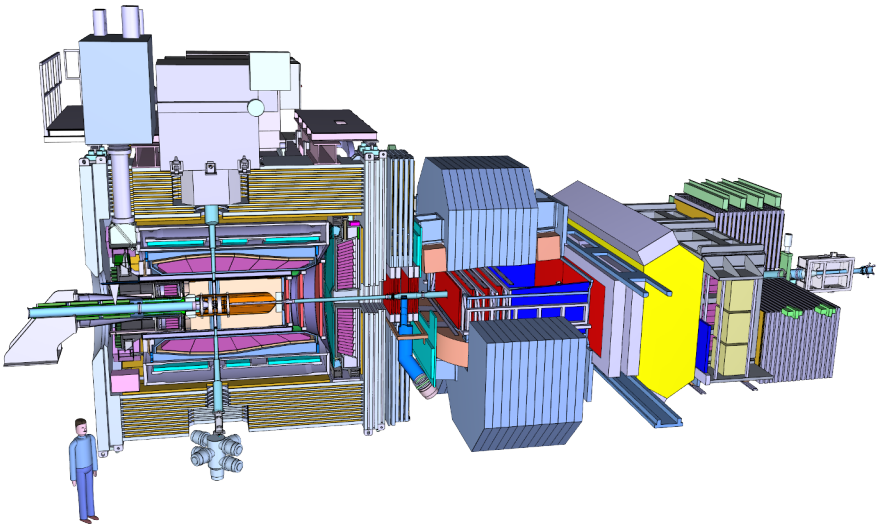

**Figure 2.** Schematic overview of the full PANDA setup. The antiproton beam will run from left to right, and the target jets/pellets from top to bottom. The left part of the detector surrounds the interaction point and is the Target Spectrometer, whereas the right part is the Forward Spectrometer.

### 3.3 Advantages of PANDA

PANDA has several advantages compared to currently operating or planned facilities:

- The production cross sections of hyperon-antihyperon final states are generally large in antiproton-proton annihilations [15]. This results in large production rates.
- Multi-strange hyperons and antihyperons can be produced in two-body reactions, which makes the kinematics simple and the dynamics straight-forward to parameterise.
- The momentum range covers the full multi-strange hyperon spectrum.
- The symmetric hyperon-antihyperon final state enables better control of systematics.
- The near $4\pi$ acceptance allows for exclusive reconstruction which minimises background.

## 4 Hyperon topics in PANDA

The combination of the PANDA features mentioned in Section 3.3 opens up for a plenty of hyperon physics topics that are difficult to study elsewhere. Two main fundamental questions, *i.e.* QCD in the confinement domain and the matter-antimatter asymmetry of the Universe, manifest themselves in different aspects of the nucleon. By utilising hyperons as a diagnostic tool, we address these questions through four research topics: hyperon production, hyperon spectroscopy, hyperon structure and hyperon decays. This is illustrated in Fig. 3.

### 4.1 Hyperon Production

The production of strange hyperons probe the strong interaction the confinement domain, as pointed out in Section 2. For a coherent understanding of the strong interaction, studies of exclusive hyperon-antihyperon production are crucial. The large amount of high-quality data on single-strange hyperons provided by the PS185 collaboration in the 1990 [15, 16] resulted in an extensive development of theoretical models. These were either based on quark-gluon degrees of freedom [17], kaon exchange [18] or a combination of the two [19]. In particular, spin observables are proven to be sensitive to the production mechanism. While most models can explain basic features such as the total cross section and the scattering angle distribution, no model was able to completely describe the spin structure of the studied reactions [15, 20]. It would be illuminating to see how spin observables such as polarisation and spin correlations behave in the multi-strange sector. However, so far only a few bubble-chamber events have been found for $\Xi^-$ and $\Xi^0$ production in $\bar{p}p$ annihilations [21]. Triple-strange hyperon production has not been observed at all in $\bar{p}p$ and the same is true for single-charmed hyperons. Measurements of the spin structure of $\overline{p}p \to \overline{Y}Y$ for ground-state multi-strange and single-charmed hyperons can serve as important guidance for the development of models for strangeness production, which in turn can shed light on the strong interaction in this energy domain.

The remarkably large production cross sections for various hyperons in $\overline{p}p \to \overline{Y}Y$ [15] imply that we can collect large hyperon samples also with the initial modest luminosity. Previous simulation studies, using a simplified Monte Carlo framework, have shown promising results regarding efficiency and background reduction [22–24]. Recently, more realistic simulation studies have been performed for single- and double strange hyperons. These simulations were performed using the PandaROOT framework, with ideal pattern recognition and particle identification. Additional selection criteria were applied that mimic the effects from a full, realistic implementation.

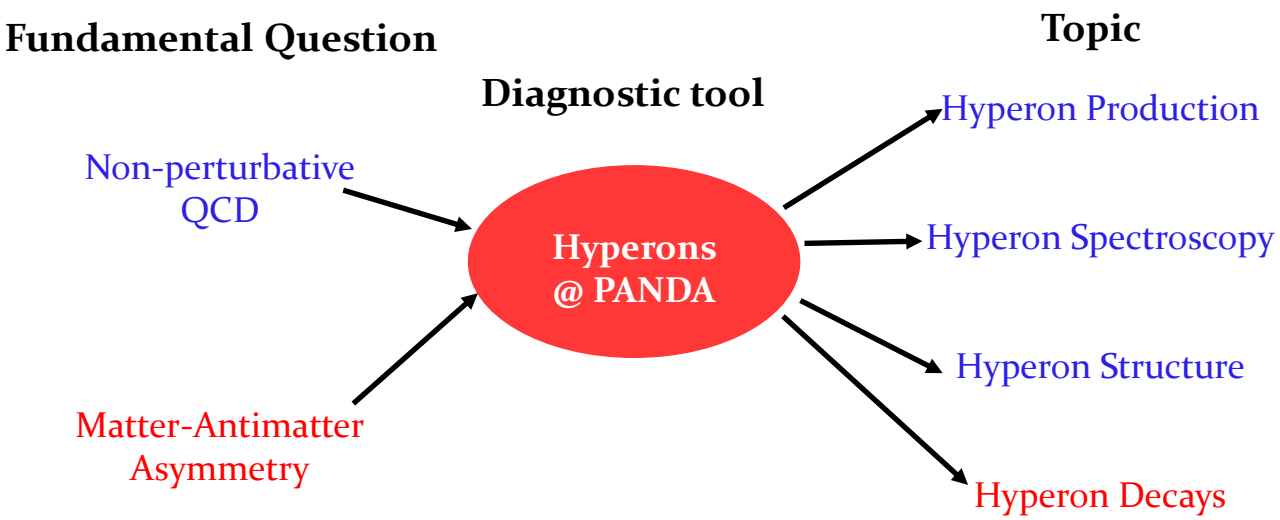


**Figure 3.** Conceptual map of hyperon physics in PANDA. It shows how the two over-arching fundamental questions (left) can be approached by a common diagnostic tool, *i.e.* hyperons (middle), from which the different subtopics emerge (right).

- $\overline{p}p \to \overline{\Lambda}\Lambda, \bar{\Lambda} \to \bar{p}\pi^+, \Lambda \to p\pi^-$ at $p_{beam}$ = 1.64 GeV/c [25]
- $\overline{p}p \to \overline{\Sigma}^0\Lambda, \bar{\Sigma}^0 \to \bar{\Lambda}\gamma, \bar{\Lambda} \to \bar{p}\pi^+, \Lambda \to p\pi^-$ at $p_{beam}$ = 1.77 GeV/c and 6.0 GeV/c [26].
- $\overline{p}p \to \overline{\Xi}^+\Xi^-, \bar{\Xi}^+ \to \bar{\Lambda}\pi^+, \bar{\Lambda} \to \bar{p}\pi^+, \Xi^- \to \Lambda\pi^-, \Lambda \to p\pi^-$ at $p_{beam}$ = 4.6 GeV/c and 7.0 GeV/c [25].

All channels include intermediate $\Lambda$ and $\bar{\Lambda}$, that were identified by combining the reconstructed final state pions and protons/antiprotons. Vertex fits and mass window criteria were applied to select good $\Lambda$ and $\bar{\Lambda}$ candidates. The background was further reduced by requiring the decay vertex to be displaced by a certain distance from the interaction point. To identify $\bar{\Sigma}^0$, the $\bar{\Lambda}$ candidates were combined with final state photons. The $\bar{\Lambda}\Lambda$ and $\bar{\Sigma}^0\Lambda$ final states were finally identified by applying a four-constraint fit. The $\Xi^-/\bar{\Xi}^+$ candidates were obtained by combining $\Lambda/\bar{\Lambda}$ candidates by pions that do not originate from a $\bar{\Lambda}\Lambda$ decay. A decay tree fitter was then applied to the full sequential decay of the $\Xi^-$ and $\bar{\Xi}^+$ hyperons. The resulting signal efficiencies are given in Table 1 and show that also at the reduced Phase One luminosity of $10^{31}\mathrm{cm}^{-2}\mathrm{s}^{-1}$, the exclusive hyperon reconstruction rates will be high. This, in combination with the estimated low background level, demonstrates the potential of PANDA as a hyperon factory.

### 4.2 Hyperon Spectroscopy

Baryon excitation spectra provide a different angle to the strong interaction. In particular, they address the question about how the forces between the quarks bind them together into baryons. Are quark degrees of freedom relevant or should baryons rather be described in terms of *e.g.* di-quark/quark configurations? Does baryon-meson dynamics play a role? Are there exotic states, such as pentaquarks and dibaryons? Hyperons address the additional question of SU(3) flavour symmetry. It is interesting to compare the findings from world-wide efforts in $N^*$ and $\Delta$ spectroscopy [29, 30], such as missing resonances and level ordering, with those of the single-strange sector. In particular, the lightness of the $\Lambda(1405)$ is difficult to explain in terms of the simple Constituent Quark Model but has instead been suggested to be a molecular state, see *e.g.* Ref.[31]. It would be illuminating to see how these observations carry over to the double- and triple strange hyperon spectra. However, the existing data bank is very scarce. Only one excited $\Xi$ state and no excited $\Omega$ states are considered well established, *i.e.* labeled with $***$ or $****$ within the PDG classification scheme. In fact, even for the ground state $\Xi$ and $\Omega$, the parity has not been determined experimentally. Furthermore, the spin determination of the $\Omega$ relies on assumptions on the $\Xi_c$ and $\Omega_c$ spin [32].

Whereas current baryon spectroscopy addresses either light-, single-strange, charmed or bottom baryons, there is a gap to fill in the multi-strange sector. PANDA is an excellent candidate to fill this gap thanks to the large foreseen hyperon production rates, the possibility of producing multi-strange hyperons in two-body reactions and the symmetric hyperon-antihyperon conditions. Recent, dedicated simulation studies on $\Xi^*(1690)$ and $\Xi^*(1820)$ production, presented by J. Pütz at this conference, demonstrates the excellent prospects of the multi-strange hyperon spectroscopy programme with PANDA [33].

### 4.3 Hyperon Structure

For nucleons, there are several ways to study structure in both soft and hard processes. In the soft region, Electro-

**Table 1.** Results from simulation studies of the various production reactions of ground state hyperons [25, 26]. The efficiencies are for exclusive reconstruction, *i.e.* considering all final state particles. The $S/B$ denotes signal-to-background ratio and the asterisk * the upper limit of a 90% confidence interval.

| $p_{\overline{p}}$ (GeV/$c$) | Reaction | $\sigma$ ($\mu$b) | Eff (%) | Decay | S/B | Rate ($s^{-1}$) at $10^{31}\mathrm{cm}^{-2}\mathrm{s}^{-1}$ |
|---|---|---|---|---|---|---|
| 1.64 | $\overline{p}p \to \overline{\Lambda}\Lambda$ | 64.0 [16] | 15.7 [25] | $\Lambda \to p\pi^-$ | 114 [25] | 44 |
| 1.77 | $\overline{p}p \to \overline{\Sigma}^0\Lambda$ | 10.9 [16] | 5.3 [26] | $\Sigma^0 \to \Lambda\gamma$ | $> 11^*$ [26] | 2.4 |
| 6.0 | $\overline{p}p \to \overline{\Sigma}^0\Lambda$ | 20.0 [27] | 6.1 [26] | $\Sigma^0 \to \Lambda\gamma$ | 21 [26] | 5.0 |
| 4.6 | $\overline{p}p \to \overline{\Xi}^+\Xi^-$ | 1.0 [28] | 8.2 [25] | $\Xi^- \to \Lambda\pi^-$ | 274 [25] | 0.3 |
| 7.0 | $\overline{p}p \to \overline{\Xi}^+\Xi^-$ | 0.3 [28] | 7.9 [25] | $\Xi^- \to \Lambda\pi^-$ | 165 [25] | 0.1 |

Magnetic Form Factors (EMFFs) quantify the inner, dynamical structure. Elastic lepton-nucleon scattering gives access to the space-like EMFFs, as shown to the left in Fig. 4. Here, the interpretation is fairly intuitive: the form factors are related to the charge- and magnetization densities [34]. Unfortunately, since hyperons are unstable, they are unfeasible as beams or targets and thus difficult to study in elastic scattering. As a consequence, the space-like region is hard to access experimentally. Instead, the time-like form factors constitute the most viable structure observables for hyperons [35]. They can be studied in various processes shown to the right of the $y$-axis in Figure 4. From the measured time-like form factors, the more intuitive space-like quantities (*e.g.* charge- and magnetisation densities) can be calculated using dispersion relations [36]. Time-like EMFFs can be complex with a relative phase, reflecting the existence of intermediate states. This phase polarises the hyperons, even if the initial state is unpolarised [37].

The time-like region covers two distinct parts with respect to the momentum transfer squared, $q^2$, of the virtual photon:

- The high-$q^2$ part, explored when an $e^+e^-$ pair annihilates to form a baryon-antibaryon pair ($e^+e^- \to B_1\bar{B}_2$, see rightmost part of Fig. 4). This region covers $q^2 > (m_{B_1} + m_{B_2})^2$.
- The low-$q^2$ part, probed in baryon Dalitz decays ($B_1 \to B_2\, e^+e^-$, see middle-left part of Fig. 4) and covering $q^2 < (m_{B_1} - m_{B_2})^2$.

If $B_1 = B_2$, the form factors are *direct*, and if $B_1 \neq B_2$ they are *transition* form factors.

So far, only a few experimental studies of hyperon structure exist. The vast majority are carried out in the high-$q^2$ part. Cross section measurements were performed by BaBar [38], CLEO-c [39] and BESIII [40] and the complete time-like structure was pinned down for the first time in a recent measurement by BESIII [41]. Some structure observables of the charmed $\Lambda_c^+$ has been extracted by Belle [42] and BESIII [43].

The low-energy region ($\approx$ 200 MeV) is rather unexplored territory. Low-energy quantities, such as magnetic and charge radii, are unknown for most ground-state hyperons [9] and the same holds for the transition form factors, that can be accessed in Dalitz decays. A pioneering measurement in the non-strange baryon sector was recently reported by the HADES collaboration for $\Delta^+(1232) \to \gamma^* p \to e^+e^- p$ [44]. In the strange sector, the only existing measurement is the weak branching fraction of the $\Xi^0 \to \Lambda e^+e^-$ decay that was found to be of the order $10^{-6}$ [45].

The major challenge in studying hyperon Dalitz decays is the small predicted branching fractions, which are typically within $10^{-3}$ - $10^{-6}$. However, the expected large hyperon production rates in PANDA can compensate for the small branching fractions. For example, the simulations in Table 1 show that at 6 GeV/$c$, $\bar{\Sigma}^0$ hyperons can be reconstructed at a rate of 5 events per second. This corresponds to $\approx$ 400 000 events per day. Provided the reconstruction efficiency of $\bar{\Sigma}^0 \to \bar{\Lambda}e^+e^-$ is of the same order of magnitude as $\bar{\Sigma}^0 \to \bar{\Lambda}\gamma$, even the branching fraction predicted by QED of $10^{-3}$ would mean that a fairly large data sample could be collected within a few weeks. This enables a test of one of the most long-standing QED predictions from Ref. [46], as well as a study of the $q^2$-dependence of the magnetic form factor $|G_M|$. The latter is related to one of the low-energy constants of the $\chi PT$ Lagrangian [7].

Thanks to an upgrade of the HADES detector [47], including forward tracker planes from PANDA, hyperon Dalitz decay studies can be undertaken already during *FAIR Phase 0* [48].

### 4.4 Hyperon Decays

According to today's paradigm, equal amounts of matter and antimatter were created in the Big Bang. However, according to all observations, our visible Universe consists mostly of matter. Where did the antimatter go? The dynamical enrichment of matter with respect to antimatter is called *Baryogenesis* [1]. It is only possible if the following criteria are fulfilled: i) processes exist which violate baryon number conservation ii) there are reactions in which charge conjugation (C) and charge conjugation and parity (CP) symmetry are violated and iii) the processes in i) and ii) occurred outside thermal equilibrium.

CP violation is incorporated in the SM by the Cabibbo-Kobayashi-Maskawa mechanism [49]. In the meson sec-

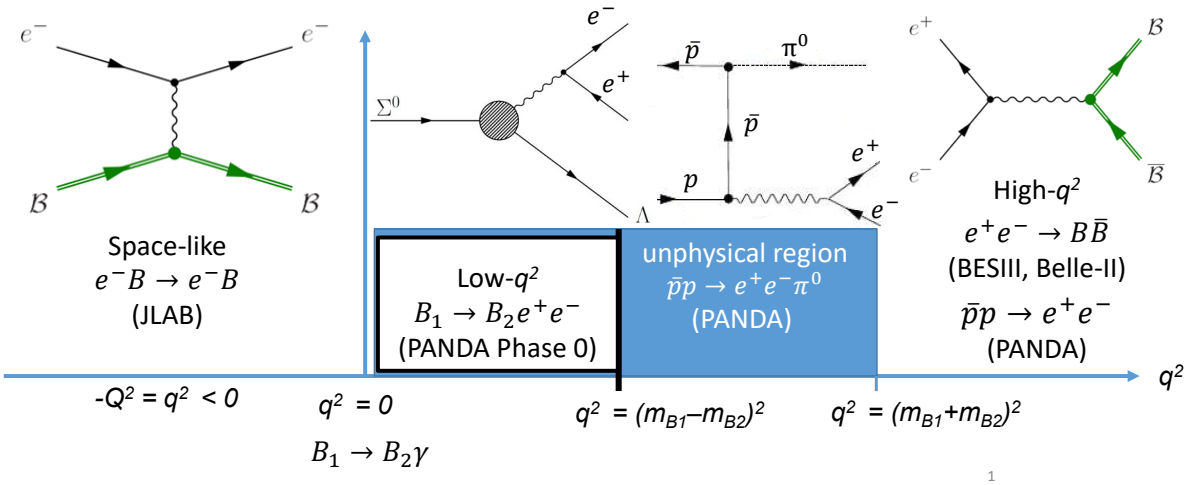


**Figure 4.** Processes for extracting EMFF in the space-like (left) and time-like (right) region. The low-$q^2$ ($4m_e^2 < q^2 < (m_{B1} - m_{B2})^2$) part of the time-like region is studied by Dalitz decays, the unphysical region ($4m_{\pi 0}^2 < q^2 < (m_{B1} + m_{B2})^2$) by $\bar{p}p \to e^+e^-\pi^0$ and the high-$q^2$ region ($q^2 > (m_{B1} + m_{B2})^2$) by $B\bar{B} \leftrightarrow e^+e^-$. Note that the unphysical region is only accessible for protons.

tor, it is established since long by experimental observations of $K^0$ and $B^0$ decays. Very recently, the LHCb collaboration reported the first evidence of CP violation in decays of the charmed $D$ meson [50]. However, our visible Universe consists largely of spin carrying baryons, for which the situation is very unclear. The only indication of CP violation observed so far for baryons was observed in the four-body decay of the bottom $\Lambda_b$ hyperon in LHCb [51]. The deviation is consistent with the SM. In total, no CP violating effects beyond the SM have ever been seen neither in the meson nor in the baryon sector. Furthermore, all deviations are too small to explain the observed matter-antimatter asymmetry of the Universe. Indeed, baryogenesis requires physics beyond the Standard Model [52].

The strange baryon sector is interesting since Super-Symmetry (SuSy) [53] predicts CP violating effects that are one to two orders of magnitudes larger than in the SM [54]. Precise measurements of hyperon decays can therefore distinguish these. Furthermore, strange hyperons decay predominatly into two-body states for which CP-odd observables are straight-forward to define. CP conservation means that particles and antiparticles decay in the same way, but with inverted spatial coordinates. Hence for a weak, two-body hyperon decay, the asymmetry parameter $\alpha$ in Eq. 1 should be the same as the $-\bar{\alpha}$ of the corresponding antihyperon. Then one can define

$$A_{CP} = \frac{\alpha + \bar{\alpha}}{\alpha - \bar{\alpha}}, \qquad (2)$$

for which a non-zero value indicates CP violation [8].

In the case of multi-strange hyperons, *e.g.* the $\Xi^-$, the sequential weak decays provide access to the additional decay asymmetry parameters $\beta$ and $\phi$. From $\beta$ and $\bar{\beta}$, the asymmetries $B_{CP}$, $B'_{CP}$ and $\Delta\phi$ can be defined in a similar manner as for $A_{CP}$ in Eq. 2. These are more sensitive to CP violation by a factor of 100 and 10, respectively [55].

The most precise experimental CP test for strange baryons so far is provided by the HyperCP experiment at Fermilab and concerns the sequential decay of the double-strange $\Xi^-$ hyperon [56]. The most precise measurement for the $\Lambda$ hyperon was recently achieved by the BESIII collaboration [57]. However, to test the SM and beyond SM theories, the precision needs to be improved by several orders of magnitude. This can be achieved in the third phase of PANDA, when the HESR has reached its design luminosity.

Hyperon-antihyperon ($Y\bar{Y}$) pair production from $p\bar{p}$ annihilations provides a clean environment for CP tests compared to the meson sector, since no mixing occurs between the $Y$ and the $\bar{Y}$. The large production rates in $p\bar{p}$ annihilations ensure excellent statistical precision. With the design luminosity of $2 \cdot 10^{32} cm^{-2} s^{-1}$, and the efficiencies of Table 1, $10^7 - 10^8$ exclusive $\bar{\Lambda}\Lambda$ events can be collected within one day. For $\bar{\Xi}^+\Xi^-$ pairs, the corresponding number is $10^5 - 10^6$. This means that PANDA has potential to reach the sensitivities required for putting SM, as well as theories beyond SM, at test.

## 5 Spin formalism in binary hyperon reactions

The weak decay of ground-state hyperons give access to spin variables, as demonstrated in Eq. 1. We have briefly discussed how this can be utilised in studies of the production mechanism, the structure and symmetry tests of the decay. Taking the full, joint decay chain into account also provides additional information in spectroscopy studies.

Hyperons produced in strong (*e.g.* $\bar{p}p$ annihilations) and electromagnetic (*e.g.* $e^+e^-$) with unpolarised beam(s) and targets can be polarised along the normal ($y_\Lambda$ in Fig. 5) of the decay plane. In addition, the spin of the hyperon is correlated with that of the antihyperon. The polarisation and spin correlations, *i.e.* the *spin variables*, are related to the production and are therefore reaction specific functions of the CMS energy and the hyperon scattering angle. The number of spin variables depend on the spin of the produced hyperons.

For the $e^+e^- \to \bar{Y}Y$ reaction, vector exchange (either virtual photon or a vector resonance, *e.g.* $J/\Psi$) dominates the production process. For spin 1/2 hyperons, the joint angular distribution of the full process, including the subsequent hyperon decays, can be expressed in terms of two production parameters. In Ref.[58], the angular distribution parameter $\eta$ and the phase $\Delta\Phi$ are chosen. These are *global* in the sense that they do not depend on the hyperon scattering angle. Equivalent global parameterisations are *s*- and *d* partial waves, spin flip or non-flip amplitudes, or electric and magnetic form factors. Due to this simple feature of the $e^+e^- \to \bar{Y}Y$ production mechanism, the spin variables have a well-defined dependence on the hyperon scattering angle. The cross section depends on five measurable quantities. In Ref. [58] these are chosen to be the hyperon scattering angle in the CMS system and the helicity angles of the proton and antiproton from the hyperon and antihyperon decays. This multi-dimensional approach is nearly model-independent, since the only assumption is that the process is dominated by vector exchange, and maximises the use of measured information. As a consequence, the statistical precision for a given sample size is increased. The method was utilised in a recent measurement by the BESIII collaboration in a precision measurement of the $\Lambda$ decay asymmetry parameters [57] and in the first complete measurement of the $\Lambda$ time-like structure [41]. The formalism has been extended to include also sequentially decaying spin 1/2 hyperons [60, 61] and spin 3/2 baryons [62].

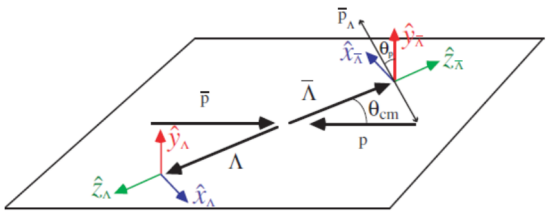


**Figure 5.** The reference system of the $\bar{p}p \to \bar{Y}Y$ reaction.

The $\bar{p}p \to \bar{Y}Y$ reaction occurs through contributions from many different amplitudes. The angular dependence of the spin variables can therefore not be parameterised in terms of global parameters as in the $e^+e^-$ case but need to be measured and compared to theory predictions. In the case of a spin 1/2 hyperon $Y$ (antihyperon $\bar{Y}$) produced in $\bar{p}p \to \bar{Y}Y$ and decaying into a spin 1/2 baryon $B$ (antibaryon $B$) and a meson $M$ (antimeson $\bar{M}$), the angular distribution of the decay baryon and antibaryon can be parameterised at each hyperon scattering angle $\cos\theta_Y$:

$$I(\theta_B, \theta_{\bar{B}})_{\theta_Y} = N[1 + \alpha \sum_i P^Y_{i,\theta_Y} \cos\theta_{Bi} + \bar{\alpha} \sum_j P^{\bar{Y}}_{j,\theta_Y} \cos\theta_{\bar{B}j} + \alpha\bar{\alpha} \sum_{ij} C^{Y\bar{Y}}_{ij,\theta_Y} \cos\theta_{Bi}\theta_{\bar{B}j}] \quad (3)$$

where $i, j = x, y, z$. With the unpolarised beam and target foreseen with PANDA and the reference system defined in Fig. 5, most spin variables must be zero due to parity conservation. The only non-zero spin variables are $P^Y_y$, $P^{\bar{Y}}_y$, $C^{Y\bar{Y}}_{xz}$, $C^{Y\bar{Y}}_{zx}$, $C^{Y\bar{Y}}_{xx}$, $C^{Y\bar{Y}}_{yy}$ and $C^{Y\bar{Y}}_{zz}$ [22, 63]. Of these, only five are independent since $P^Y_y = P^{\bar{Y}}_y$ and $C^{Y\bar{Y}}_{xz} = C^{Y\bar{Y}}_{zx}$.

The $\bar{p}p \to \bar{\Omega}^-\Omega$ reaction is more complicated; assuming it is correct that the $\Omega$ has spin 3/2, it has fifteen polarisation parameters $r^L_M(\cos\theta_\Omega)$, where $L = 0, 1, 2, 3$ and $M = 0, \pm1, \pm2, \pm3$. Three of these can be accessed in the $\Omega$ decay [22], the other four can be accessed through the sequential decay chain $\Omega \to \Lambda K^-, \Lambda \to p\pi^-$, and similarly for $\bar{\Omega}^+$ [64, 65]. From the full decay chain, structure obsevables such as form factors can be determined, as well as fundamental properties such as spin.

Most existing Partial Wave Analysis (PWA) frameworks for baryons consider decay processes. However, by including the weak sequential decay chain of ground state hyperons, it should be possible to extract more information from the available data, provided the samples are large enough. Previous chapters have demonstrated the potential of the various PANDA phases in this regard and the development of combined, model-independent framework will further enhance the physics scope of PANDA.

## 6 Acknowledgement

The author is grateful for the support by the local organisers of NSTAR 2019, the Swedish Research Council (No. 2013-04278) and the Knut and Alice Wallenberg foundation, Sweden (No. 2016.0157).

## References

[1] A. D. Sakharov, Pisma Zh. Eksp. Teor. Phys. Fiz. **5**, 32 (1967).
[2] C. A. Aidala *et al.,* Rev. Mod. Phys. **85**, 655 (2013).
[3] S. Scherer and M. R. Schindler, Lect. Notes Phys. **830**, 1 (2012).
[4] G. A. Miller, Phys. Rev. Lett. **99**, 112001 (2007).
[5] R. Pohl *et al.,* Nature **466** (2010) 213; C. E. Carlson, Prog. Part. Nucl. Phys. **82**, 59 (2015).
[6] N. Bezginov *et al.,* Science **365**, Issue 6457, 1007-1012 (2019).
[7] C. Granados, S. Leupold and E. Perotti, Eur. Phys. J. **A 53**, 17 (2017).
[8] I. I. Bigi, A. I. Sanda, *CP violation* Cambridge Monographs on Particle Physics, Nuclear Physics and Cosmology, **vol. 9**, Cambridge University Press (2000).
[9] M. Tanabashi *et al.,* Phys. Rev. D **98**, 030001 (2018).
[10] T. D. Lee and C. N. Yang, Phys. Rev. **108**, 1645 (1957).
[11] The PANDA Collaboration, PANDA Technical Progress Report, FAIR-ESAC (2005).
[12] S. Spataro *et al.*, *The PandaRoot framework for simulation,reconstruction and analysis*, J. Phys.: Conf. Ser. **331**, 032031 (2011).
[13] M. Al-Turany *et al.*, *The FairRoot Framework*, J. Phys.: Conf. Ser. **396**, 022001 (2012).
[14] R. Brun and F. Rademakers, *ROOT - An Object Oriented Data Analysis Framework*, Nucl. Inst. Meth. in Phys. Res. A **389**, 81-86 (1997).

[15] T. Johansson, *Proceedings of LEAP 2002* 95 (2003).
[16] P. D. Barnes *et al.* Nucl. Phys. A **526**, 575 (1991);P. D. Barnes *et al.* Phys. Rev. C **62**, 055203 (2000);K. D. Paschke *et al.*, Phys. Rev. C **74**, 015206 (2006).
[17] M. Kohno and W. Weise, Phys. Lett. B **179** 15 (1986); H. R. Rubinstein and H. Snellman Phys. Lett. B **165** 187 (1985); S. Furui and A. Faessler, Nucl. Phys. A **486** 669 (1987); M. Burkardt and M. Dillig Phys. Rev. C **37** 1362 (1988); M. A. Alberg *et al.* Z. Phys. A **331** 207 (1988).
[18] F. Tabakin and R. A. Eisenstein Phys. Rev. C **31** 1857 (1985); M. Kohno and W. Weise, Phys. Lett. B. **179** 15 (1985); P. La France *et al.* Phys. Lett. B **214** 317 (1988); R. G. E. Timmermans *et al.* 1992 Phys. Rev. D **45** 2288 (1992); J. Haidenbauer *et al.* Phys. Rev. C **46** 2516 (1992).
[19] P. G. Ortega *et al.* Phys. Lett. B. **696** 352 (2011).
[20] E. Klempt, F. Bradamante, A. Martin, J.-M. Richard, Phys. Rep. **368**, p 119 (2002).
[21] B. Musgrave and G. Petmezas, Nuovo Cim. **35**, 735 (1965);C. Baltay *et al.,* Phys. Rev. B **140**, 1027(1965).
[22] E. Thomé, *Multi-Strange and Charmed Antihyperon-Hyperon Physics for PANDA*
Ph. D. Thesis, Uppsala University (2012).
[23] The PANDA collaboration, Physics Performance Report (2009).
[24] S. Grape, *Studies of PWO Crystals and Simulations of the* $\overline{p}p \to \overline{\Lambda}\Lambda, \overline{\Lambda}\Sigma^0$ *Reactions for the PANDA experiment*
Ph.D. Thesis, Uppsala University (2009).
[25] W. Ikegami-Andersson, *Exploring the Merits and Challenges of Hyperon Physics with PANDA at FAIR*, PhD Thesis, Uppsala University (2020).
[26] G. Perez Andrade, *Production of the* $\Sigma^0$ *hyperons in the PANDA experiment at FAIR*, Master thesis, Uppsala University (2019).
[27] H. Becker *et al.,* Nucl. Phys. B **141**, 48 (1978).
[28] A. B. Kaidalov and P. E. Z. Volkovitsky, Phys. C **63** 51 (1994).
[29] E. Klempt and J. M. Richard, Rep. Prog. Phys. **82** 1095 (2010).
[30] V. Crede and W. Roberts, Rep. Prog. Phys. **76** 076301 (2013).
[31] J. M. M. Hall *et al.,* Phys. Rev. Lett. **114**, 132002 (2015).
[32] B. Aubert *et al.* (BaBar Collaboration), Phys. Rev. Lett. **97**, 112001 (2006).
[33] J. Puetz, these proceedings (2019).
[34] V. Punjabi *et al.,* Eur. Phys. J. A **51**, 79 (2015).
[35] S. Pacetti *et al.,* Phys. Rep. **550-551**, 1 (2015).
[36] M. A. Belushkin et al., Phys. Rev. C **75** 035202 (2007).
[37] A. Z. Dubnickova *et al.*, Nuovo Cim. A **109** 241 (1996).
[38] B. Aubert *et al.* (BaBar Collaboration), Phys. Rev. D **76**, 092006 (2007).
[39] S. Dobbs *et al.,* Phys. Lett. B **739**, 90 (2014); S. Dobbs *et al.,* Phys. Rev. **D 96**, 092004 (2017).
[40] M. Ablikim *et al.*(BESIII Collaboration), Phys. Rev. D **97**, 032013 (2018).
[41] M. Ablikim *et al.* (BESIII Collaboration), Phys. Rev. Lett. **123**, 122003 (2019).
[42] G. Pakhlova *et al.,* Phys. Rev. Lett. **101**, 172001 (2008).
[43] M. Ablikim *et al.* (BESIII Collaboration), Phys. Rev. Lett. **120**, 132001 (2018).
[44] J. Adamczewski-Musch *et al.,* Phys. Rev. C **95**, 065205 (2017).
[45] J. R. Batley *et al.,* Phys. Lett. B **650**, 1 (2007).
[46] J. Bernstein *et al.,* Phys. Rev. **139**, 1650 (1965);G. Feldman and T. Fulton, Nucl. Phys. **8**, 106 (1958).
[47] G. Agakishiev *et al.,* Eur. Phys. J. A **41**, 243 (2009).
[48] J. Adamczewski-Musch *et al.,* Proposal for experiments at SIS18 during FAIR Phase 0 (2017).
[49] M. Kobayashi and T. Maskawa, Prog. Theor. Phys. **49**, 652 (1973); N. Cabibbo, Phys. Rev. Lett. **10** (1963) 531.
[50] R. Aaij (LHCb collaboration), Phys. Rev. Lett. **122**, 211803 (2019)
[51] R. Aaij (LHCb collaboration), Nature Phys. **13**, 391 (2017).
[52] L. Canetti *et al.,* New J. Phys. **14**, 095012 (2012).
[53] X.-G. He *et al.,* Phys. Rev. D **61**, 071701 (2000).
[54] J. Tandean *et al.,* Phys. Rev. D **67**, 056001 (2003).
[55] J. F. Donogue *et al.,* Phys. Rev. D **74** 3927 (1995).
[56] HyperCP Collaboration, Phys. Rev. Lett. **93** 262001 (2004).
[57] M. Ablikim *et al.* (BESIII Collaboration), Nature Phys. **15**, p. 631–634 (2019).
[58] G. Fäldt and A. Kupsc, Phys. Lett. B **772**, 16 (2017).
[59] G. Fäldt, Phys. Rev. D **97**, 053002 (2018).
[60] G. Fäldt and K. Schönning, *Sequential hyperon decays in the reaction* $e^+e^- \to \Sigma^0\bar{\Sigma}^0$, arXiv:1908.04157 (2019).
[61] P. Adlarson and A. Kupsc, *CP symmetry tests in the cascade-anticascade decay of charmonium*, arXiv:1908.03102 (2019).
[62] E. Perotti *et al.,* Phys. Rev. D **99**, 056008 (2019).
[63] K. D. Paschke *et al.,* Phys. Rev. C **74**, 015206 (2006).
[64] K. Schönning and E. Thomé, J. Phys. Conf. Ser. 556, 012007 (2014).
[65] E. Perotti, J. Phys. Conf. Ser. **1024** no.1, 012019 (2018).